Modeling the thermalization of electrons in conditions relevant to atmospheric pressure He-O_2 nanosecond pulsed discharges

M. S. Bieniek, J. L. Walsh, M. I. Hasan[a]
Centre for Plasma Microbiology,
Department of Electrical Engineering and Electronics,
The University of Liverpool,
Liverpool, L69 3GJ, UK
[a] email *mihasan@liverpool.ac.uk*

Abstract

The electron thermalization process is significant in nanosecond pulsed discharges due to the applied voltage pulse's short duration and rapid rise and fall times. In this contribution a comparison was made between two approaches to modeling the electron kinetics of electron thermalization in atmospheric pressure helium plasma with an oxygen admixture. Modeling based on the direct solution of the local time-dependent electron Boltzmann equation was compared with modeling based on the commonly used but less general local mean energy approximation. For modeling based on the local time-dependent electron Boltzmann equation, a temporary faster decay in the population of electrons in the high energy tail, and a slower decay in the population of intermediate energy electrons was observed while the electron swarm cooled from an average energy of above 8 eV, without an electric field present. During that period, the electron impact reaction rate coefficients of helium direct ionization and electronic excitation decreased by more than 3 orders of magnitude as compared to the modeling based on the local mean energy approximation. Global modeling of the evolution of plasma species densities in response to an electric field typical of atmospheric pressure pulsed discharges was performed with the two approaches to electron kinetics. Differences in the species densities were observed between the two approaches, with an 100% increase in the maximum density of electrons found with the modeling based on the local mean energy approximation.

1 Introduction

Pulsed discharges are interesting from the point of view of fundamental science as, for example, one may greatly exceed the self-sustaining voltage threshold whilst maintaining stability. They can operate in multiple discharge modes, including a large volumed diffuse mode where they efficiently generate reactive species [1]. They also form on or in liquids [2, 3]. Pulsed discharges are interesting in applied science, where, for example, they are studied in the fields of ignition and combustion of hydrocarbon fuels [4], and plasma medicine [5]. They are of particular

interest in applied science as they have been demonstrated to have high stability and be more energy efficient at generating radicals than discharges based on a sinusoidally varying voltage [6]. A summary of literature on pulsed discharges may be found in the review papers by Brandenburg et al, and Wang and Namihira [1, 7].

The electron thermalization time, defined as the time taken for the macroscopic electron swarm characteristics (e.g. electron impact reaction rate coefficients, average electron energy, electron mobility, etc) to reach a steady state after an electric field is instantaneously altered, was observed to be as long as hundreds of nanoseconds in simulations of atmospheric pressure low temperature xenon plasma [8]. In pulsed discharges, applied voltages may vary by thousands of volts over a period of nanoseconds [7], and as the variation of the electric field may occur on time scales shorter than the electron thermalization time, pulsed discharges can consequently include a population of unthermalized electrons.

In an early review paper by Shizgal et al. [9], four major theoretical approaches to the study of the thermalization of electrons in gases were identified. These being, (1) the displaced-pseudo Maxwellian approach, where the electron distribution function is assumed to be Maxwellian and parameterised by the time dependent electron temperature, yielding a simple equation for the evolution in time of the average electron energy; (2) Monte Carlo collision simulations, which in principle may be very accurate but are also computationally costly; (3) the Boltzmann equation written in the form of a Fokker-Plank equation, and solved as an Eigenvalue problem, allowing calculations of the electron velocity distribution functions, and some averaged quantities such as the electron mobility, average electron energy, and thermalization times; and (4) the electron degradation theory, based on the Spencer-Fano equation, an equation for the balance of the electron density for a particular energy range. The review reports calculations which utilized these approaches, to solve for the electron thermalization time in Helium, as well as the evolution of key swarm parameters. A striking theoretical prediction from the Fokker-Plank approach was, in gases with a Ramsauer–Townsend minimum, transient negative electron mobility can occur, a finding that was later verified experimentally [10]. A general description, however, of the evolution of the electron velocity distribution function, considering inelastic collisions, and heating of the electrons by the background gas, was not readily computationally available using these approaches. Modeling of the electron thermalization process by means of the direct solution of the time-dependent electron Boltzmann equation, using the now well known two-term approximation, was later demonstrated to be both sufficiently general and computationally inexpensive [11]. Solutions found using helium electron impact cross sections were first reported by Bronic and Kimura [12]. Modeling was performed of the evolution of electron swarms, from various Gaussian initial electron energy distribution functions (EEDF), cooling where no electric field was present. The thermalization time was found to be 80 ns, and scaled proportionally with the density of the background gas. No specific structures on the EEDF were identified for the unthermalized electrons. Modeling of the electron thermalization process by means of solution of the multi-term time-dependent electron Boltzmann equation were also reported using helium cross sections around the same time, and compared to the two-term treatment [13]. Large differences in the reaction rate coefficients were observed while electron swarms were cooling through high average energies (> 15 eV). Trunec et al. reported the effect of electron-electron collisions on electron swarm thermalization using the time-dependent electron Boltzmann equation with the two-term approximation with Helium cross sections [14]. As the discharge ionization degree was increased, the cooling swarm's EEDF became increasingly Maxwellian in shape, and shorter thermalization times were found. Modeling of the electron thermalization process by means of the solution to the multi-term time-dependent electron

Boltzmann equation was recently published by Boyle et al. [8]. In the report, the electron thermalization process in xenon was described for electrons heated by a large range of electric fields, and for the cooling of the electron swarms as the field was removed. The thermalization time in the heating phase was found to depend on the applied field strength.

The thermalization of electron swarms in pulsed discharges is regularly modelled using the local mean energy approximation (LMEA) (e.g. as in [15–20]). This assumes macroscopic electron swarm characteristics vary only with the local average electron energy. Where the local average electron energy is usually determined by solving an equation for the electron energy density flux, with rate and transport coefficients determined with the solution of the local steady state Boltzmann equation [21]. The time-dependent term in the Boltzmann equation is *a priori* excluded from this approach, leaving only the EEDF found at steady state considered.

In this work the thermalization of electron swarms were modelled responding to instantaneously altered electric fields (to be consistent with other work on the theory of electron thermalization; e.g. [8]), in atmospheric pressure helium plasma with an oxygen admixture. The electron kinetics were determined by means of the direct solution of the local time-dependent electron Boltzmann equation with the two term approximation (TDEBE), and by means of the LMEA. Macroscopic electron swarm characteristics were generated, and used to compare the two approaches to electron kinetics. Transient structures on unthermalized EEDF were identified and analyzed. Global modeling of the evolution of plasma species densities in response to a time varying electric field typical of atmospheric pressure pulsed discharges experiments, was performed with the two approaches to electron kinetics. The species densities were analyzed, and the validity of the commonly used LMEA approach to modeling such discharges was investigated.

The outline of this paper is as follows. In Sec. 2 the model used and numerical implementation are described. In Sec. 3 the results of the modeling are described and discussed. The findings are summarised and conclusions are drawn in Sec. 4.

2 Model and numerics

2.1 Numerical model

The equations used in this work were derived from the electron Boltzmann equation, using the two-term approximation, as described by Raizer [22]. A term was included for the heating of the electrons by the background gas (the dominant form of heating at very low electric fields). The inelastic collisions were written in the form described by Hagelaar and Pitchford [21], and converted into velocity space. The resultant equation one finds solves for the electron velocity distribution function:

$$v^2\frac{\partial f_0}{\partial t}+\frac{\partial}{\partial v}[-\frac{e^2E}{3m_e^2}\frac{v^2}{V_m}\frac{\partial f_0}{\partial v}-\frac{x_kNk_bTv^3\sigma_m}{M_k}\frac{\partial f_0}{\partial v}-x_k\frac{m_e}{M_k}V_mv^3f_0]=v^2Q_{inel} \tag{1}$$

where

$$Q_{ion}=-\sum_i x_k[V_i(\varepsilon)f_0(\varepsilon)-\frac{v(\varepsilon+E_i)}{v}V_i(\varepsilon+E_i)f_0(\varepsilon+E_i)+\int_0^\infty \delta V_i(E_i)f_0(E_i)d\varepsilon]; \tag{2}$$

$$Q_{ex} = -\sum_{ex} x_k[V_{ex}(\varepsilon)f_0(\varepsilon) - \frac{v(\varepsilon + E_{ex})}{v}V_{ex}(\varepsilon + E_{ex})f_0(\varepsilon + E_{ex})]; \tag{3}$$

$$Q_{at} = -\sum_{at} x_k[V_{at}(\varepsilon)f_0(\varepsilon)] \tag{4}$$

and $Q_{inel} = Q_{ion} + Q_{ex} + Q_{at}$; $V_r = x_k N v \sigma_r(\varepsilon)$; and the subscript r denotes each reaction, of type m for momentum transfer, type i for ionization, ex of excitation, and at for attachment reactions; e is the elementary charge; E is the electric field; x_k is the mole fraction of target particle k; f_0 is the isotropic part of the electron velocity distribution function; v is the electron velocity; σ is the electron impact cross section; ε is the electron energy; k_b is the Boltzmann constant; m_e is the mass of an electron; M_k is the mass of target particles and T is their temperature; δ is the Kronecker delta function; E_i and E_{ex} are, respectively, the ionization and excitation potentials for each excitation and ionization reaction. SI units are used except in the case of electron energies which are in electron volts.

It is assumed by eqs.(1)-(4) that the primary electron takes all of the energy after an ionizing collision. This assumption was justified as the alternate limiting case, where the energy of the primary and secondary electrons is shared evenly after an ionizing collision, was also implemented, and no significant differences were found between the two approaches as electron swarms cooled from energies above 10 eV (the thermalization process of most interest in this article).

The assumptions used in the derivation become invalid in the following discharge conditions [22]: (1) When the electric field is very strong. If a collision causes an electron to lose a considerable fraction of its energy, the electron motion becomes directed mostly along the axis of the electric field, and so far from being isotropic, invalidating the two term approximation. This can happen when an electron gains more energy than is needed for the excitation or ionization of the background gas in one mean free path: $eEl > I$. Where l is the electron mean free path and I is the energy threshold for ionization. (2) When the field frequency is very high. The derivation assumed the electric field is almost constant over the period of time in which several electron-neutral collisions occur. This is the so-called "DC" condition, where RF heating is not considered, which, in cases where elastic collisions dominate and inelastic collisions are negligible, holds for angular electric field frequencies with $\omega << \frac{2m_e}{M_k}\nu_m$. Where ν_m is the electron collisional frequency; ω is the angular field frequency. In an atmospheric pressure Helium plasma this is the case below around 25 Mhz. (3) When the field varies over short distance. The derivation assumes that the electric field does not vary much over the distance of the electron energy spectrum relaxation length, which, in cases where elastic collisions dominate and inelastic collisions are negligible is: $\Lambda_u = v_D \tau_u \approx v_D \frac{M_k}{2m_e \nu_m}$. Where v_D is the electron drift velocity and τ_u is the electron energy spectrum relaxation time. In atmospheric pressure helium plasma, under a 100 Td strength reduced electric field, $\Lambda_u \approx 0.5$ mm. (4) When the ionization degree is high. The derivation did not take into account electrons colliding with other electrons. This is the case for high ionization degrees, $\frac{n_e}{N} > 1 \times 10^{-4}$. The authors note that each of these assumptions are questionable for certain discharge conditions, but that it was outside of the scope of the presented modeling work to investigate what the physical consequences of these would be.

The macroscopic electron swarm characteristics were calculated using the definitions described by Hagelaar and Pitchford in [21], and are as follows. The electron mobility multiplied by the background gas density was calculated as:

$$\mu N = -\frac{\gamma}{3}\int_0^\infty \frac{\varepsilon}{Q}\frac{\partial f_0}{\partial \varepsilon}d\varepsilon,$$

the electron impact rate coefficients:

$$k_k = \gamma\int_0^\infty \varepsilon\sigma_k f_0 d\varepsilon,$$

and the mean electron energy:

$$<\varepsilon>=\int_0^\infty \varepsilon^{3/2} f_0 d\varepsilon,$$

where γ is the constant coefficient, $\sqrt{\frac{2e}{m^e}}$; and Q is the effective total momentum-transfer cross section.

The definition of the thermalization time used in this work is the time taken to reach within 10% of the steady state value of the average electron energy, when being heated by an instantaneously applied electric field, or when cooling after a field is instantaneously removed. This definition is used in order to be consistent with earlier work on the thermalization of electron swarms in Helium [12, 14].

2.2 Model validation

The numerical model, Eqs.(1)-(4), was solved using the commercial finite element analysis software COMSOL Multi-physics. The implementation was validated by comparing its stationary solutions to those generated by the Boltzmann equation solver 'Bolsig+' [21].

The temporal evolution computed from Eqs.(1)-(4) was validated by comparing results with, the computationally expensive, Monte Carlo Collision (MCC) simulations. The MCC simulations were implemented following the formulation by Ristivojevic and Petrovic [23]. A swarm of electrons thermalized under an applied field of a strength of 50 Td were released in atmospheric pressure helium with no electric field present. Newton's second law was solved for every particle while time was advanced in time-steps of size 3×10^{-12} s. As electrons approached helium atoms, the MCC code simulated a reaction type based on the incident electron's energy. The evolution in time of the electron swarm's average energy was calculated.

The same set of reactions and cross sections, those from the Phelps database [24], were used in the simulations performed with Bolsig+, Eqs.(1)-(4), and the MCC simulations. Figure 1 shows a comparison of the average electron energy computed by each simulation approach.

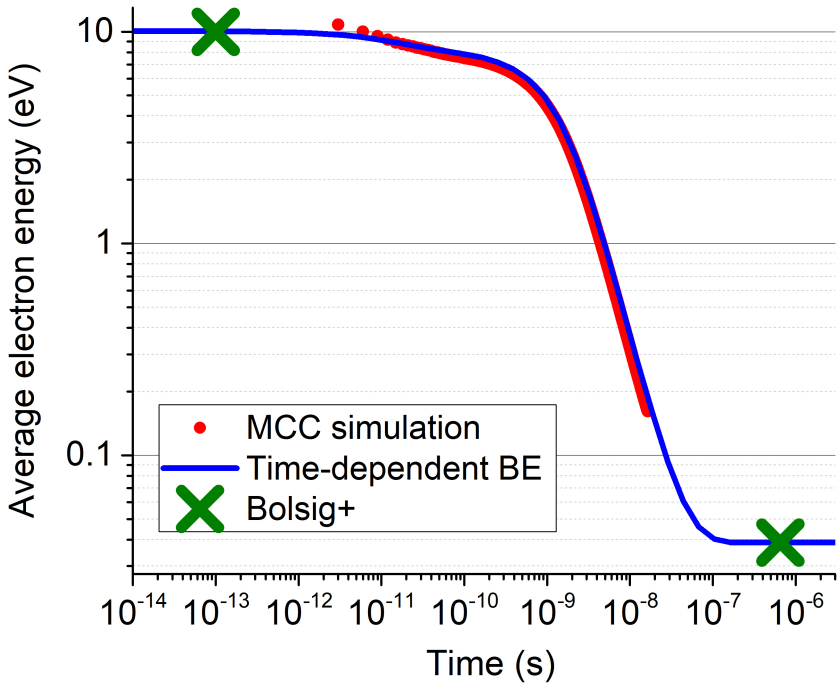

Figure 1. Evolution in time of the average electron energy of an electron swarm cooling in atmospheric pressure Helium, without an electric field present. Calculated using: time-dependent electron Boltzmann equation solver (solid line), Monte Carlo Collision simulation (dashed line). Bolsig+, solutions for 50 Td, and 0 Td, plotted in time near the initial and final conditions, respectively, of the modeling with the time-dependent Boltzmann equation (crosses).

The EEDF generated with BOLSIG+ exactly matched those generated in steady state conditions with Eqs.(1)-(4). Good agreement was found between the MCC simulation results and the results generated from the modeling based on the solution of the TDEBE, as seen in Figure 1. The trend was of better agreement with smaller time steps in the MCC simulations, which were gradually reduced down to 3×10^{-12} s, progressively leading to longer simulation times (of more than one week). This, at least in part, being a consequence of a momentum-transfer collision frequency of less than 1×10^{12} Hz at high energies.

2.3 Electron impact reaction kinetics and the global model

The kinetic scheme for the transfer of electron energy by electron impact reactions is described in Table 1, for atmospheric pressure helium with a 0.1% oxygen admixture. With oxygen included only as an admixture, the vibrational excitation of O_2 does not significantly effect the EEDF, and so for the sake of simplicity was not included in this work.

Reaction number	Reaction	Energy exchange	Ref.
R1	$e + He \rightarrow He + e$	calculated	[24],[25]
R2	$e + He \rightarrow He^* + e$	19.8 eV	[24],[25]

R3	$e + He \rightarrow 2e + He^+$	24.58 eV	[24],[25]
R4	$e + O_2 \rightarrow e + O_2$	calculated	[24],[25]
R5	$e + O_2 \rightarrow 2e + O_2^+$	12.06 eV	[24],[25]
R6	$e + O_2 \rightarrow e + 2O$	6.1 eV	[24],[25]
R7	$e + O_2 \rightarrow e + O + O(^1D)$	8.04 eV	[24],[25]
R8	$e + O_2 \rightarrow O + O^-$	6.26 eV	[24],[25]
R9	$e + O_2 \rightarrow e + O_2(a^1\Delta)$	0.98 eV	[24],[25]

Table 1. Kinetic scheme for electron energy transfer by electron impact in atmospheric pressure He-O_2 plasma.

Calculations of the electron swarm parameters were made with the EEDF generated from Eqs.(1)-(4).

Results obtained using the LMEA approach adopted Eq.(5) for calculating the average electron energy, for given electric fields [26]. As in the derivation of Eqs.(1)-(4), the density of electrons was assumed to be constant in space and time, allowing one to solve for the electron swarm energy without coupling the problem to the plasma species densities:

$$\frac{d\varepsilon}{dt} = e\mu_e E^2 - 3\frac{m_e}{M_k}\nu_{en}(T_e - T_g) - r_j n_k \Delta H_j; \tag{5}$$

where ε is the average electron energy, μ_e is the electron mobility, ν_{en} is the electron-neutral momentum transfer frequency, r_j is the reaction rate coefficient for each direct electron impact reaction j, ΔH_j is the corresponding collisional energy loss. The electron swarm parameters, including those in Eq.(5), were calculated using the stationary form of Eqs.(1)-(4), solved for a given average electron energy simultaneously with Eq.(5).

The electron swarm parameters obtained by the aforementioned methods were, in turn, incorporated into a regular global model. The global model comprised of a set of species continuity equations, with source terms added describing the recombination of charged species at the vessel walls:

$$\frac{dn_i}{dt} = R_i - \frac{A}{V}\sqrt{\frac{kT_e}{M_i}}n_i; \tag{6}$$

$$\frac{dn_e}{dt} = R_e - \frac{A}{V}\sqrt{\frac{kT_e}{m_e}}n_e; \tag{7}$$

$$\frac{dn_{ex,r,n}}{dt} = R_{ex,r}; \tag{8}$$

$$\frac{dn_{i_g}}{dt} = R_{i_g} + \frac{A}{V}\sqrt{\frac{kT_e}{M_{i_g}}}n_{i_g} \tag{9}$$

where R is the reaction rate, n is the species density, A is the discharge vessel wall area and V is the discharge vessel volume. The subscripts ex, r, and n refer to each excited, radical, and neutral species, respectively; g refers to the ground state of a corresponding ion species. The terms in Eqs.(6)-(9) describing the losses of charged species to the vessel walls have the

temperature of electrons set to 1 eV, in order to allow a greater focus on the variations of the discharge species reaction kinetics. The vessel modelled was cylindrical with a radius of 50 cm and a height of 50 cm. The vessel was large so that reactions in the bulk were mostly unaffected by losses of to the walls.

The plasma reaction scheme used is described in [27], with the reactions involving nitrogen and hydrogen excluded. For the sake of simplicity, the excited oxygen species were essentially instantly converted to their ground states. The details are presented in the appendix.

3 Results and discussion

The thermalization times of electron swarms, in helium plasma under atmospheric pressure, with a 0.1% admixture of oxygen, are plotted in Figure 2. For the heating phase of the electron swarm, the initial condition of the steady state solution to Eqs.(1)-(4), where there is no electric field, was used. An electric field, whose strength is on the y-axis of the figure, was instantaneously applied and the simulations were run until a new steady state was reached. For the cooling phase, the initial condition was the steady state solution for a constant electric field whose strength is stated on the y-axis. The electric field was instantaneously removed, and the evolution in time was modelled until another steady state was reached.

The thermalization times for the cooling phase matches other work on helium, of around 80 ns [12]. No dependence on the initial EEDF was observed for the thermalization times in the cooling phase. The thermalization times in the heating phase show a notable dependence on the applied electric field strength, as in work on xenon [8].

The thermalization times in the heating and cooling phases are noticeably different. This difference was principally attributed to the different kinetic processes undergone while the electron swarms approached their steady states. In the cooling phase, electrons increasingly lose less energy through collisions with the background gas as their average energy falls. The electrons approach thermal equilibrium with the background gas through elastic collisions. In the heating phase, where the electron swarm is heated by the electric field, the steady state is approached at high average electron energies. At high average electron energies, electrons experience inelastic collisions, which are very effective energy loss channels. For example, an electron loses 24.58 eV in a single ionizing collision with Helium, while it would take hundreds of elastic collisions for the electron to lose the same amount of energy. The increased energy lost at high average electron energies to inelastic collisions reduces the number of collisions required before a steady state is reached, resulting in faster thermalization times in the heating phase as compared to the cooling phase.

The same thermalization times were found when performing modeling using the LMEA (Eq.(5)), and by direct solution of the TDEBE (Eqs.(1)-(4)).

When the electric field varies on time scales less than the thermalization time, e.g. for an electric field reducing faster than 50 Td per 80 ns, an account of the electron thermalization process should be made (and so the local field approximation should be avoided).

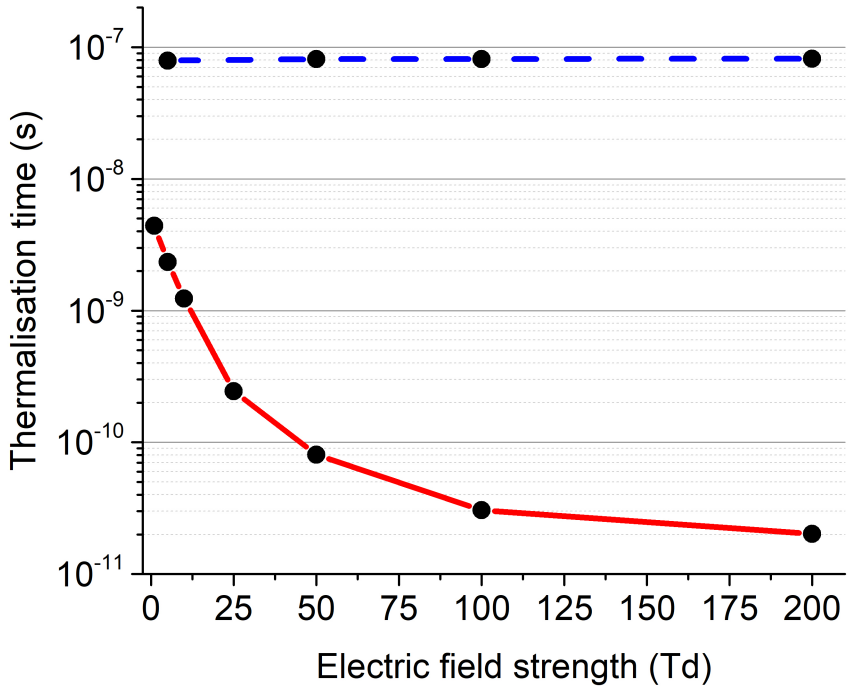

Figure 2. Field dependence of thermalization times of electrons in atmospheric pressure helium with 0.1% oxygen admixture. Solid red line: heating thermalization times; initial conditions of thermalized electrons in no field, with instantaneously applied electric field with strength shown on y-axis. Dashed blue line: cooling thermalization times; initial conditions of thermalized electrons in electric field of strength shown on y-axis, when field instantaneously removed. T = 300 K.

The evolution in time of the average electron energy of an electron swarm, cooling without an electric field present, from the steady state caused by an electric field of strength 100 Td, is plotted in Figure 3 a). The modeling was performed using the LMEA, and also by direct solution of the TDEBE. Between 50 picoseconds and 500 picoseconds, an increase in the average electron energy, of more than 1.5 eV, was found when modeling using the more physically accurate TDEBE, as compared to the LMEA. The increase was seen, during the same period of time, and of around 1.5 eV in difference, when cooling from higher energies. The origins of this hump are discussed later in this section.

Only very small differences in the average electron energy were observed when comparing the two approaches in the heating phase, or when cooling from energies of 4 eV and below, as seen in Figure 3 b).

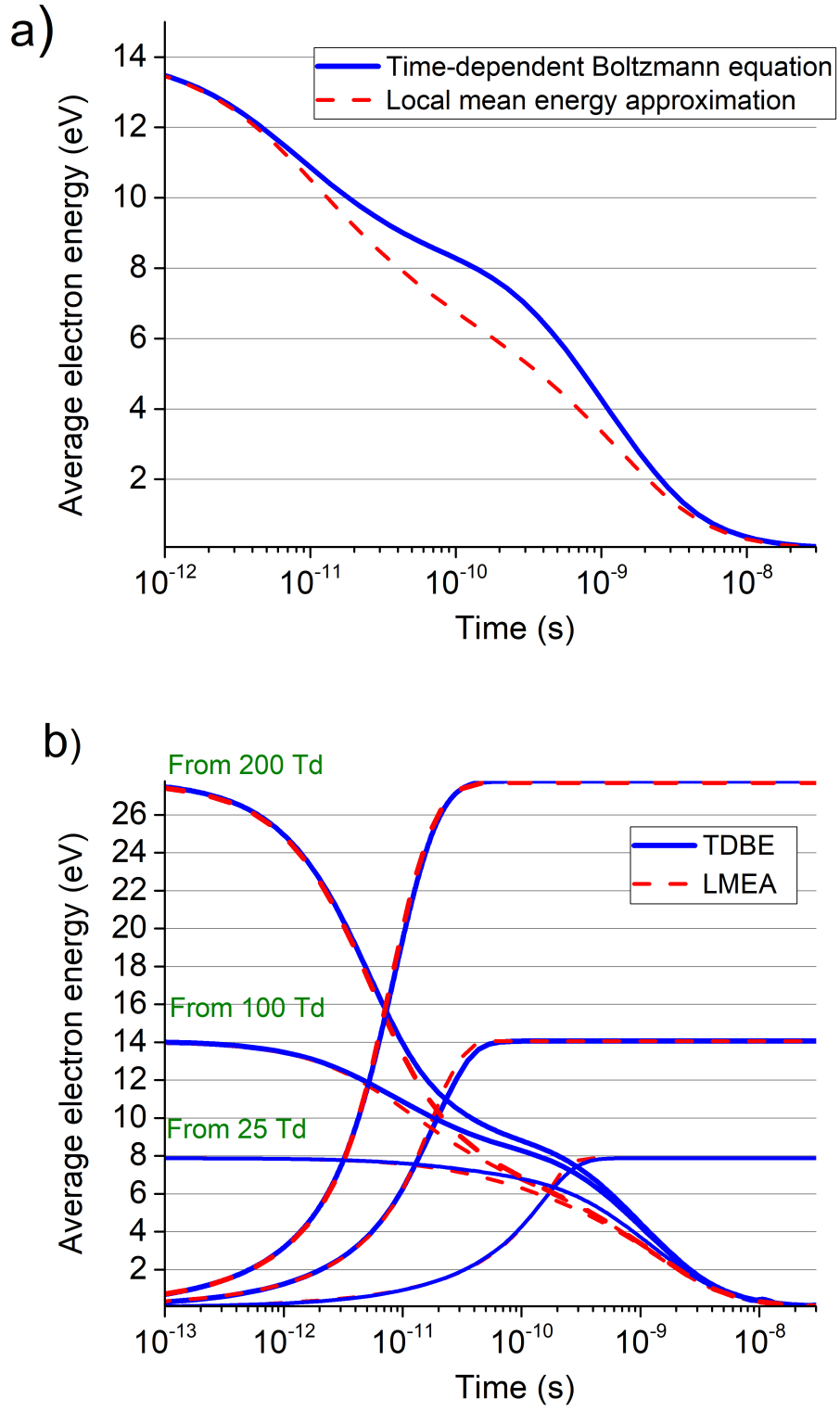

Figure 3. The time evolution of the average electron energy for an electron swarm a) cooling under no electric field, from the steady state caused by an 100 Td strength electric field, and b) heated to and cooling from the steady states caused by a 25 Td, 100 Td, and a 200 Td strength electric field. Solid line: time-dependent electron Boltzmann equation. Dashed line: using local mean energy approximation. T = 300 K.

The evolution in time of the EEDF, under the conditions used to obtain Figure 3, are plotted in Figure 4. Notable differences in the structure of the EEDF were observed between the two approaches. For each time plotted, modeling using the TDEBE gave a reduced high energy tail. As can be seen in Figure 4, a ledge formed in energy space, with a swell on its low energy side, as compared to the modeling using the LMEA. In other words, the TDEBE model predicted a temporary faster decay in the population of hot electrons, and a slower decay in the population of warm electrons as compared with modeling based on the LMEA. The transient structures in energy space were attributed to electronic excitation of helium causing the scattering out of electrons from the high energy end of the distribution function, into lower energy space, which is further discussed later. The steep ledge in energy space was formed at around 20 eV, from 0.1 ns. As time progressed, the ledge became less steep and moved down in energy space. During the period plotted, fewer electrons had between 0.1 and 1.5 eV in the unthermalized EEDF.

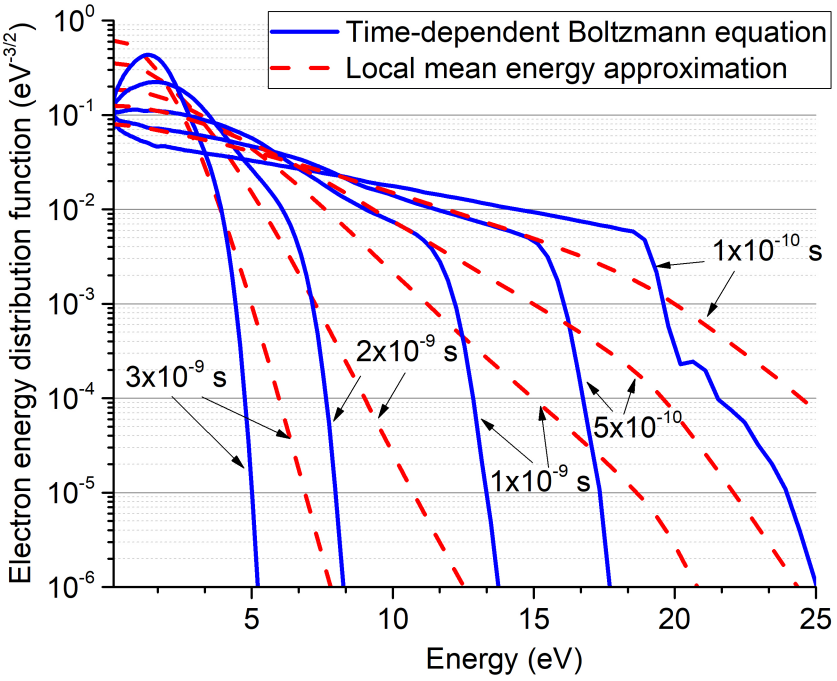

Figure 4. The EEDF used when modeling electron swarms cooling under no electric field, from the steady state caused by a 100 Td strength electric field. Solid line: time-dependent electron Boltzmann equation. Dashed line: using local mean energy approximation.

The evolution in time of the average energy lost per electron, to a given electron impact reaction, under the conditions used to obtain Figure 3, are plotted in Figure 5. Initially, and up to 0.2 ns, the dominant channel for electron energy loss was via the electronic excitation of helium. This loss was greater in the modeling using the LMEA. This being related to the higher numbers of electrons in the high energy tail of the thermalized EEDF, seen in Figure 4. When the transient structures on the unthermalized EEDF were taken into account, a reduced number of high energy electrons were present, which led to fewer inelastic collisions, and so correspondingly fewer energy losses, and a higher average electron energy, as seen in Figure 3.

Electron energy lost via collisions with the O_2 admixture are not large enough to cause the differences observed between the EEDF computed via the LMEA and the TDEBE seen Figure 4.

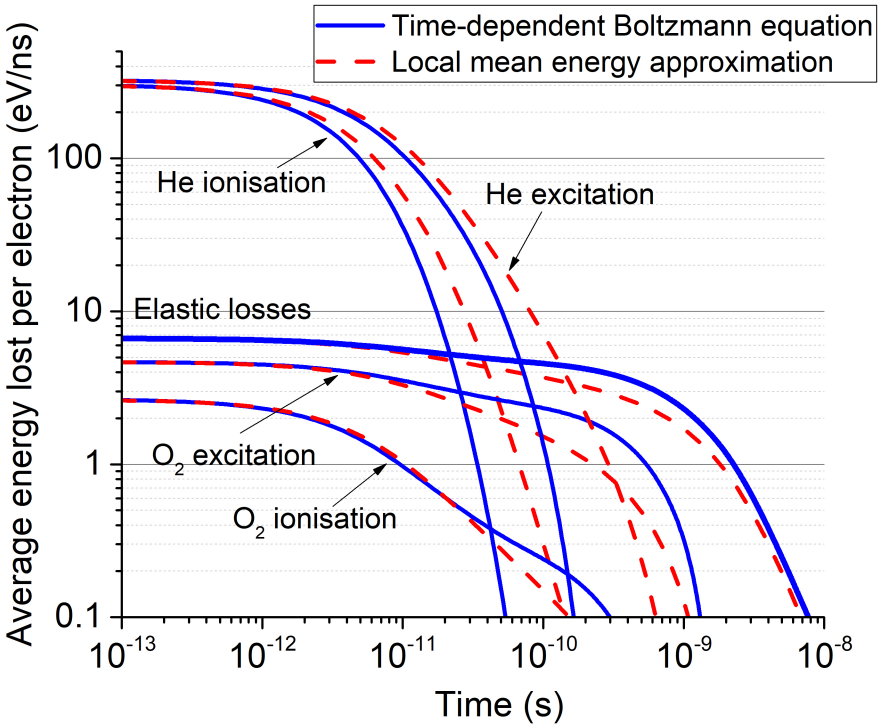

Figure 5. The evolution in time of the average energy lost per electron, for electron swarms cooling under no electric field, from the steady state caused by a 100 Td strength electric field. Solid line: time-dependent electron Boltzmann equation. Dashed line: local mean energy approximation.

The evolution in time of the electron impact reaction rate coefficients for electronic excitation and ionization of helium, and dissociation of O_2, under the conditions used to obtain Figure 3, are plotted in Figure 6. Between 0.2 and 2 nanoseconds, more than 3 orders of magnitude of difference was seen in the ionization and excitation rate coefficients, as a results of the reduced high energy tail in the unthermalized EEDF. During this time, an increase in the rate coefficient of dissociation of O_2 by direct electron impact was also observed, associated with the higher average electron energy in the unthermalized EEDF.

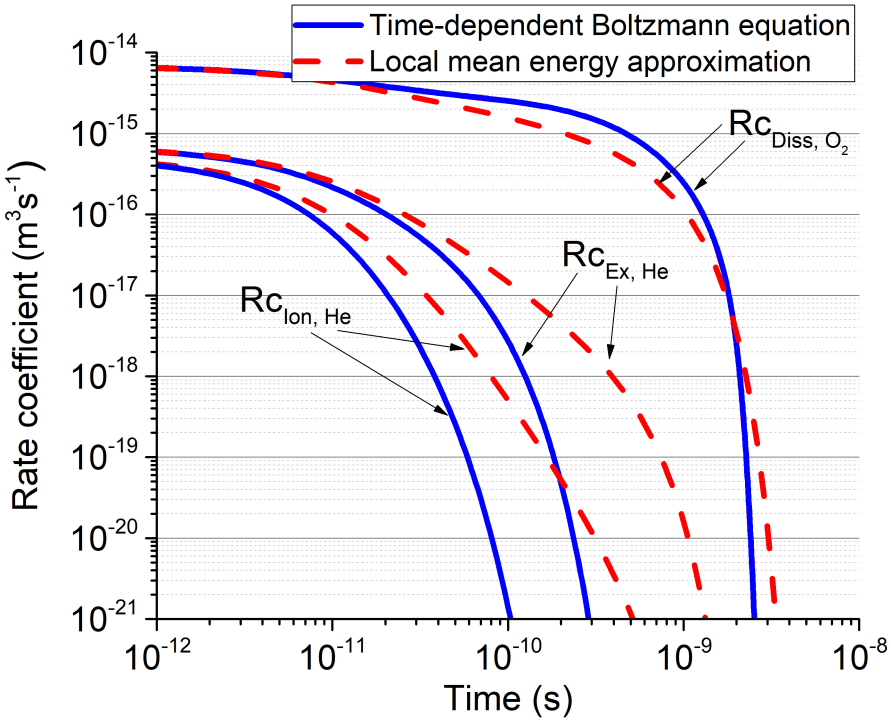

Figure 6. Rate coefficients for electron swarms cooling under no electric field, from the steady state caused by a 100 Td strength electric field. Solid line: time-dependent electron Boltzmann equation. Dashed line: local mean energy approximation.

Global modeling results of the evolution of plasma species densities in response to a pulse of electric field are plotted in Figure 7a, 7b, and 7c. Unlike in the earlier results described in this section, where changes in the electric field occurred instantaneously, here the variation of the electric field occurred as a pulse, a gradual function of time, as plotted in Figure 7a. The pulse lasted for 10 ns and had rise and fall times of 20 Td per ns. The pulse was similar to the one calculated by Popov [28], which was based on experimental data of pulsed discharges [29, 30]. The gas temperature was set to 350 K to take into account gas heating by the discharge [6].

The evolution of the number density of atomic oxygen was examined when electron kinetic parameters were determined with the LMEA approach, and by direct solution of the TDEBE. For the heating phase, and while the electric field is at its peak, the species densities were essentially the same between the two approaches. During the cooling phase, differences between the approaches began to form. After the pulse, the LMEA approach yielded a greater number density of atomic oxygen, and also at times a reduced number density of atomic oxygen as compared with the approach based on the TDEBE. The maximum difference being of around 20%. The differences demonstrated the complex interaction between plasma species densities, and the reaction rate coefficients generated by the different EEDF approaches.

In Figure 7b the evolution in time of the number density of electrons, computed with the two modeling approaches, are plotted. Similar to the case of atomic oxygen, in the heating phase and while the electric field was at its peak, the species densities were essentially the same for the two modeling approaches. After the cooling phase, the peak electron density was found to be 100% higher with the LMEA approach.

In Figure 7c the evolution in time of the density of positive ions are plotted. The two ap-

proaches to electron kinetics produced similar effects in the heating phase, as with the electrons plotted in Figure 7 a and b. For atomic helium ions the difference is observed after the heating phase, with the species density being higher with the local mean energy approximation. For some periods of time (e.g at 0.1 μs), there is more than an order of magnitude of difference in the number density of atomic helium ions between the two approaches. After the pulse the dominant ions are dioxygen ions.

Figures 7 a, b, and c show charged and radical species densities increasing after the pulse of electric field, as the electron mean energy is low. This is because dissociation and ionization reactions also occurred after the pulse of the electric field, fuelled by species generated during the pulse.

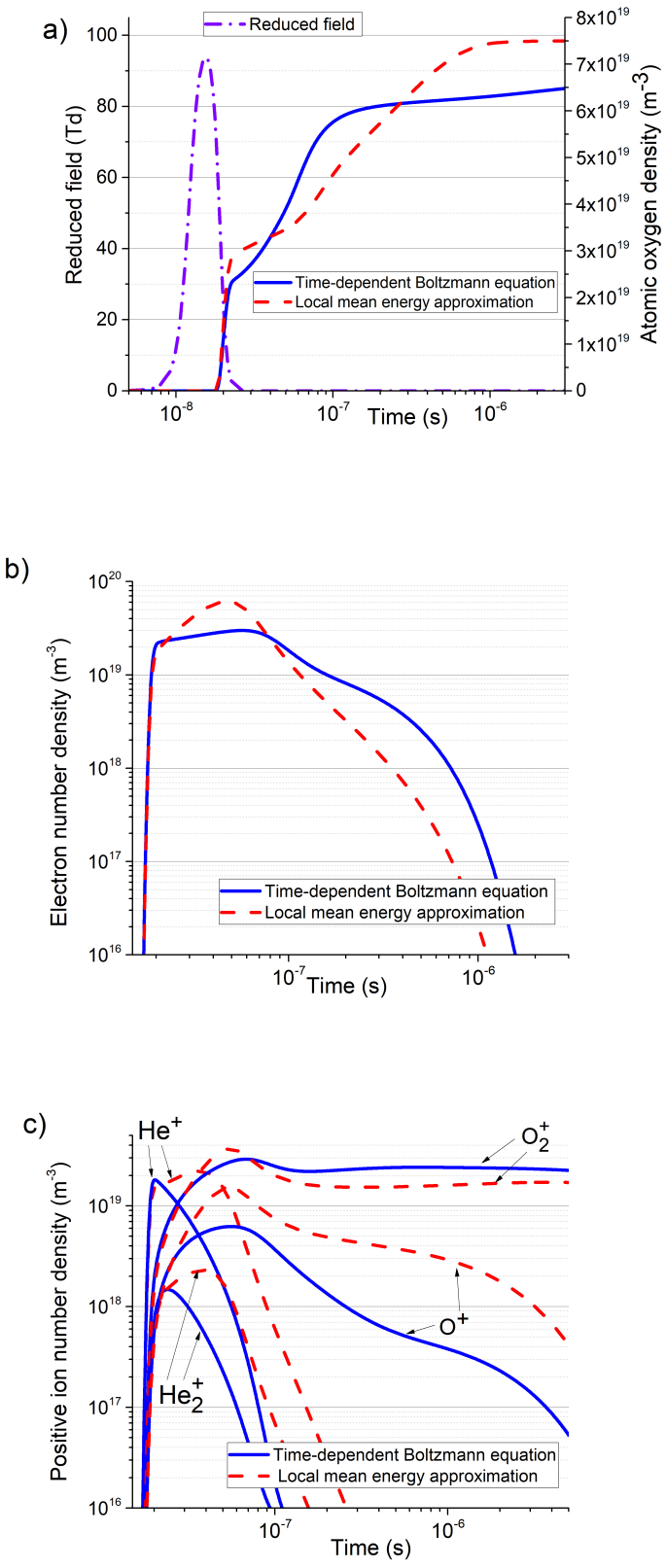

Figure 7. Global modeling of the evolution of plasma species densities in response to a pulse of electric field. a) Evolution of atomic oxygen density b) evolution of electron density c) evolution of atomic helium ion density. T=350 K.

In Figure 8 a and b the evolution in time of the three largest reaction rates are plotted for atomic oxygen production, and electron production, respectively. The conditions used were the same as were used to obtain Figure 7.

The dominant channel of atomic oxygen production during the pulse of electric field was dissociative ionization by electron impact with dioxygen. The rate was higher in the case of the TDBE approach due to the higher electron temperature during the cooling phase of the pulse. Later on, when the dominant channel of atomic production was dissociative recombination of dioxygen ions, the reduced electron density with the TDBE approach resulted in a lower rate compared with the LMEA approach. Then, when dissociative charge exchange from atomic helium ions to dioxygen was dominant, the TDBE approach resulted in a higher rate.

In the case of electron production, the largest reaction rate for the LMEA approach was of step-wise ionization of atomic helium. Modelling using the TDBE approach had dramatically less step-wise ionization, due to fewer electronically excited helium atoms produced during the cooling phase of the pulse.

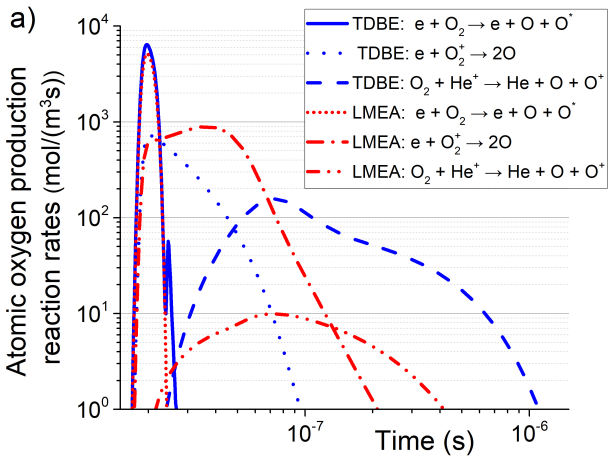

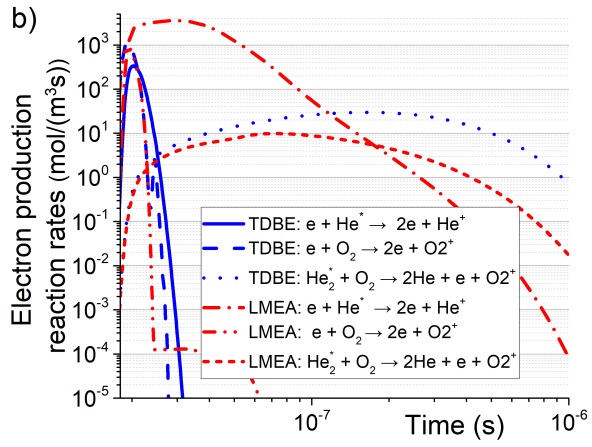

Figure 8. Evolution of the three largest reaction rates in response to a pulse of electric field for a) atomic oxygen production, and b) electron production. Solid line: time-dependent electron Boltzmann equation. Dashed line: local mean energy approximation. T=350 K.

4 Conclusions

Electron swarms were modelled being heated by a wide range of electric fields, and cooling from those heated states when no electric field was present, in atmospheric pressure helium plasma with an oxygen admixture. Modeling was performed by means of the solution of the local TDEBE, as well as by the LMEA. In the heating phase, and when cooling from average energies below 4 eV, little difference was observed between the two approaches. When cooling from above an average electron energy of 8 eV, transient structures on the EEDF were identified in the approach based on the solution to the TDEBE. A steep ledge in energy space, corresponding with a decreased number of high energy electrons, and swell before the ledge, corresponding with an increased number of middle energy electrons, between 0.1 and 3 ns, was found. The transient EEDF structures resulted in an increase in the average electron energy, and also large differences in electron impact reaction rate coefficients. Global modeling was performed to determine the effect of these transient EEDF structures on the evolution of plasma species densities under a pulse of electric field typical of pulsed discharges. For the heating phase of the pulse, and while the electric field was at its peak, the plasma species densities were essentially the same between the two approaches. During the cooling phase and in the afterglow, differences were observed in the species densities, with, for example, an around 100% increase in the maximum density of the electrons found with the modeling based on the LMEA.

The modeling indicates that for the rapid variations of the local electric field found in atmospheric pressure He-O_2 nanosecond pulsed discharges, simulations based on the local mean energy approximation, as compared to those based on, the more computationally demanding but more physically realistic, approach of the direct solution of the local two-term time-dependent electron Boltzmann equation, are not accurate while electrons are cooling after a short pulse of voltage.

Acknowledgments The authors acknowledge the support of the Engineering and Physical Science Research Council (projects EP/S025790/1, EP/S026584/1, EP/R041849/1, and EP/T000104/1).

Data availability The data that support the findings of this study are available from the corresponding author upon reasonable request.

5 Appendix

The plasma reaction kinetic scheme was sourced from [27], where reactions involving nitrogen and hydrogen were excluded. The excited oxygen species were treated as their corresponding ground state.

Reaction Number	Reaction formula	Reaction coefficient	Energy cost (eV)	Ref.
R1	$e + He \rightarrow e + He$	calculated		[24, 27]
R2	$e + He \rightarrow e + He^*$	calculated	19.8	[24, 27]
R3	$e + He^* \rightarrow e + He$	$1.7633 \times 10^{-16} \varepsilon_{avg}^{0.31}$	-19.8	[27]
R4	$e + He \rightarrow 2e + He^+$	calculated	24.58	[24, 27]
R5	$e + He^* \rightarrow 2e + He^+$	$1 \times 10^{-13} \varepsilon_{avg}^{0.6} \exp(-7.175/\varepsilon_{avg})$	4.78	[27]
R6	$e + O_2 \rightarrow e + O_2$	calculated		[24, 27]
R7	$e + O_2 \rightarrow e + O + O(1D)$	calculated	8.401	[24, 25]
R8	$e + O_2 \rightarrow e + O_2(a1\Delta)$	calculated	0.98	[24, 25]
R9	$e + O_2 \rightarrow 2e + O_2^+$	calculated	12.06	[24, 27]
R10	$e + He_2^* \rightarrow 2e + He_2^+$	$7.28 \times 10^{-16} \varepsilon_{avg}^{0.71} \exp(-5.1/\varepsilon_{avg})$	3.4	[27]
R11	$e + He_2^+ \rightarrow He + He^*$	$6.1382 \times 10^{-15} \varepsilon_{avg}^{-0.5}$		[27]
R12	$2e + He^+ \rightarrow e + He$	$7 \times 10^{-32} T_{eg}^{-4.5}$		[27]
R13	$2e + He_2^+ \rightarrow e + 2He$	$7 \times 10^{-32} T_{eg}^{-4.5}$		[27]
R14	$e + He + He_2^+ \rightarrow 3He$	$2 \times 10^{-39} T_{eg}^{-2.5}$		[27]
R15	$e + He^+ \rightarrow He$	2×10^{-18}		[27]
R16	$e + He_2^+ \rightarrow 2He$	1×10^{-14}		[27]
R17	$e + O_2^+ \rightarrow 2O$	$7.762 \times 10^{-15} \varepsilon_{avg}^{-1}$	-6.91	[27]
R18	$e + He + He^+ \rightarrow He + He^*$	1×10^{-39}		[27]
R19	$e + He + He_2^+ \rightarrow 2He + He^*$	$5 \times 10^{-39}/T_{eg}$		[27]
R20	$e + He + He_2^+ \rightarrow He + He_2^*$	1.5×10^{-39}		[27]
R21	$2e + He^+ \rightarrow e + He^*$	$6 \times 10^{-32} T_{eg}^{-4}$		[27]
R22	$2e + He_2^+ \rightarrow He + He^* + e$	$1 \times 10^{-32} T_{eg}^{-4}$		[27]
R23	$2e + He_2^+ \rightarrow He_2^* + e$	$3 \times 10^{-32} T_{eg}^{-4}$		[27]
R24	$e + He^+ \rightarrow He^*$	$6.76 \times 10^{-19 T_e - 0.5}$		[27]
R25	$e + He_2^+ \rightarrow He + He^*$	$8.9 \times 10^{-15} T_{eg}^{-1.5}$		[27]
R26	$e + O_2 \rightarrow O_2^-$	calculated		[24, 27]
R27	$2e + O_2^+ \rightarrow e + O_2$	$7 \times 10^{-32} T_{eg}^{-4.5}$		[27]
R28	$e + O_2 + O_2^+ \rightarrow 2O_2$	$2.49 \times 10^{-41} T_{eg}^{-1.5}$		[27]
R29	$e + O_3 \rightarrow O + O_2^-$	$5.87 \times 10^{-15} T_e^{-1.5} \exp(-1.59/T_e)$		[27]
R30	$e + O_3 \rightarrow O_2 + O^-$	$2.12 \times 10^{-15} T_e^{-1.06} \exp(-0.93/T_e)$		[27]
R31	$e + O^- \rightarrow O + 2e$	$5.47 \times 10^{-14} T_e^{0.324} \exp(-2.98/T_e)$	2.98	[27]
R32	$e + O_2 \rightarrow 2O + e$	calculated	6.1	[27]
R33	$e + O_2 \rightarrow O + O^-$	$1.07 \times 10^{-15} T_e^{-1.39} \exp(-6.26/T_e)$	6.26	[27]
R34	$e + He + O \rightarrow He + O^-$	1×10^{-43}		[27]
R35	$e + He + O_2 \rightarrow He + O_2^-$	$3.6 \times 10^{-43} T_e^{-0.5}$		[27]
R36	$e + He + O_3 \rightarrow He + O_3^-$	1×10^{-43}		[27]

R37	$e + O + O_2 \rightarrow O + O_2^-$	1×10^{-43}		[27]
R38	$e + O + O_2 \rightarrow O_2 + O^-$	1×10^{-43}		[27]
R39	$e + 2O_2 \rightarrow O_2 + O_2^-$	$3.6 \times 10^{-43} T_e^{-0.5}$		[27]
R40	$e + O_2 + O_3 \rightarrow O_2 + O_3^-$	1×10^{-43}		[27]
R41	$e + O^+ \rightarrow O$	4×10^{-18}		[27]
R42	$e + O_2^+ \rightarrow O_2$	4×10^{-18}		[27]
R43	$2e + O^+ \rightarrow O + e$	$7 \times 10^{-32} T_{eg}^{-4.5}$		[27]
R44	$e + He + O^+ \rightarrow He + O$	$6 \times 10^{-39} T_{eg}^{-2.5}$		[27]
R45	$e + O_2 + O^+ \rightarrow O_2 + O$	$6 \times 10^{-39} T_{eg}^{-2.5}$		[27]
R46	$e + O \rightarrow 2e + O^+$	$9 \times 10^{-14} T_e 0.7 \exp(-13.6/T_e)$	13.6	[27]
R47	$e + O_2 \rightarrow 2e + O + O^+$	$5.4 \times 10^{-16} T_e 0.5 \exp(-17/T_e)$	17	[27]
R48	$e + O_2 \rightarrow O^- + e + O^+$	$7.1 \times 10^{-17} T_e 0.5 \exp(-17/T_e)$	17	[27]
R49	$He^* + 2He \rightarrow He_2^* + He$	1.3×10^{-45}		[27]
R50	$2He + He^+ \rightarrow He + He_2^+$	1×10^{-43}		[27]
R51	$2He^* \rightarrow He + e + He^+$	2.7×10^{-16}		[27]
R52	$O_2 + He^+ \rightarrow He + O_2^+$	$3.3 \times 10^{-17} T_g^{0.5}$		[27]
R53	$He^* + He_2^+ \rightarrow 2He + He^+$	1×10^{-16}		[27]
R54	$O_2 + He_2^+ \rightarrow 2He + O_2^+$	$1 \times 10^{-15} T_g^{0.5}$		[27]
R55	$2O_2 \rightarrow 2O + O_2$	$6.6 \times 10^{-15} T_0^{-1.5} \exp(-59000/T_g)$		[27]
R56	$He^* + He + O_2 \rightarrow 2He + e + O_2^+$	1.6×10^{-43}		[27]
R57	$He^* + O_2 \rightarrow He + e + O_2^+$	2.6×10^{-16}		[27]
R58	$2O \rightarrow O_2$	$9.26 \times 10^{-40} T_0^{-1}$		[27]
R59	$3O \rightarrow O_2 + O$	$9.21 \times 10^{-46} T_0^{-0.63}$		[27]
R60	$2O + O_2 \rightarrow 2O_2$	$2.56 \times 10^{-46} T_0^{-0.63}$		[27]
R61	$O_2^- + He^+ \rightarrow O_2 + He$	$2 \times 10^{-13} T_0^{-1}$		[27]
R62	$O_2^- + He_2^+ \rightarrow 2He + O_2$	1×10^{-13}		[27]
R63	$O_2^- + O_2^+ \rightarrow 2O + O_2$	1×10^{-13}		[27]
R64	$O_2^- + O_2^+ \rightarrow 2O_2$	$4.2 \times 10^{-13} T_0^{-0.5}$		[27]
R65	$O_2^- + He + He_2^+ \rightarrow 3He + O_2$	$2 \times 10^{-37} T_0^{-2.5}$		[27]
R66	$O_2^- + O_2 + He_2^+ \rightarrow 2He + 2O_2$	$2 \times 10^{-37} T_0^{-2.5}$		[27]
R67	$He + O_2^- \rightarrow He + O_2 + e$	$3.9 \times 10^{-16} \exp(-7400/T_g)$		[27]
R68	$He^* + O_2^- \rightarrow He + O_2 + e$	3×10^{-16}		[27]
R69	$He_2^* + O_2^- \rightarrow 2He + O_2 + e$	3×10^{-16}		[27]
R70	$O_2 + O_2^- \rightarrow 2O_2 + e$	$2.7 \times 10^{-16} T_0^{0.5} \exp(-5590/T_g)$		[27]
R71	$2He^* \rightarrow e + He_2^+$	1.05×10^{-15}		[27]
R72	$He_2^* + He^* \rightarrow 2He + e + He^+$	5×10^{-16}		[27]
R73	$He_2^* + He^* \rightarrow He + e + He_2^+$	2×10^{-15}		[27]
R74	$2He_2^* \rightarrow 3He + e + He^+$	3×10^{-16}		[27]
R75	$2He_2^* \rightarrow 2He + e + He_2^+$	1.2×10^{-15}		[27]
R76	$2He + He^* \rightarrow He + He_2^*$	1.5×10^{-46}		[27]
R77	$2O + He \rightarrow O_2 + He$	1×10^{-45}		[27]
R78	$O_2 - + He + O_2^+ \rightarrow He + 2O_2$	$2 \times 10^{-37} T_0^{-2.5}$		[27]
R79	$O_2 - + O_2 + O_2^+ \rightarrow 3O_2$	$2 \times 10^{-37} T_0^{-2.5}$		[27]
R80	$He_2^* + O_2 \rightarrow 2He + e + O_2^+$	3.6×10^{-16}		[27]
R81	$O^- + He + O_2^+ \rightarrow O + O_2 + He$	$2 \times 10^{-37} T_0^{-2.5}$		[27]
R82	$O^- + O_2 + O_2^+ \rightarrow O + 2O_2$	$2 \times 10^{-37} T_0^{-2.5}$		[27]
R83	$O^- + O_2 + O_2^+ \rightarrow O_2 + O_3$	$2 \times 10^{-37} T_0^{-2.5}$		[27]

R84	$2O_3 \rightarrow O + O_2 + O_3$	$1.6 \times 10^{-15} \exp(-11400/T_g)$	[27]
R85	$O_3 + O_2 \rightarrow O + 2O_2$	$1.6 \times 10^{-15} \exp(-11400/T_g)$	[27]
R86	$O_3 + O \rightarrow 2O + O_2$	$9.4 \times 10^{-17} \exp(-11400/T_g)$	[27]
R87	$O_3 + O \rightarrow 2O_2$	$8 \times 10^{-18} \exp(-2060/T_g)$	[27]
R88	$2O + O_2 \rightarrow O_3 + O$	$3.4 \times 10^{-46} T_0^{-1.2}$	[27]
R89	$O + 2O_2 \rightarrow O_3 + O_2$	$6 \times 10^{-46} T_0^{-2.8}$	[27]
R70	$O + O_2 + O_3 \rightarrow 2O_3$	$2.3 \times 10^{-47} \exp(-1057/T_g)$	[27]
R71	$O + O_2 + He \rightarrow He + O_3$	$3.4 \times 10^{-46} T_0^{-1.2}$	[27]
R72	$O^- + O_2^+ \rightarrow 3O$	1×10^{-13}	[27]
R73	$O^- + O_2^+ \rightarrow O + O_2$	$1 \times 10^{-13} T_0^{-0.5}$	[27]
R74	$O^- + He^+ \rightarrow O + He$	$2 \times 10^{-13} T_0^{-1}$	[27]
R75	$O^- + He_2^+ \rightarrow O + 2He$	1×10^{-13}	[27]
R76	$O^- + He + He^+ \rightarrow 2He + O$	$2 \times 10^{-37} T_0^{-2.5}$	[27]
R77	$O^- + O_2 + He^+ \rightarrow He + O + O_2$	$2 \times 10^{-37} T_0^{-2.5}$	[27]
R78	$O^- + He + He_2^+ \rightarrow 3He + O$	$2 \times 10^{-37} T_0^{-2.5}$	[27]
R79	$O^- + O_2 + He_2^+ \rightarrow 2He + O + O_2$	$2 \times 10^{-37} T_0^{-2.5}$	[27]
R80	$O^- + He \rightarrow He + O + e$	$2.5 \times 10^{-24} T_0^{0.6}$	[27]
R81	$O^- + He^* \rightarrow He + O + e$	3×10^{-16}	[27]
R82	$O^- + He_2^* \rightarrow 2He + O + e$	3×10^{-16}	[27]
R83	$O^- + O \rightarrow O_2 + e$	$2 \times 10^{-16} T_0^{0.5}$	[27]
R84	$O^- + O_2 \rightarrow O + O_2^-$	1.5×10^{-18}	[27]
R85	$O^- + O_2 \rightarrow O_3 + e$	$5 \times 10^{-21} T_0^{0.5}$	[27]
R86	$O^- + O_3 \rightarrow 2O_2 + e$	$3.01 \times 10^{-16} T_0^{0.5}$	[27]
R87	$O^- + H \rightarrow OH + e$	5×10^{-16}	[27]
R88	$O_2^- + O \rightarrow O_2 + O^-$	$1.5 \times 10^{-16} T_0^{0.5}$	[27]
R89	$O_2^- + O \rightarrow O_3 + e$	$1.5 \times 10^{-16} T_0^{0.5}$	[27]
R90	$He + O_3 \rightarrow He + O + O_2$	$1.56 \times 10^{-15} \exp(-11400/T_g)$	[27]
R91	$He^* + O_3 \rightarrow He + O + e + O_2^+$	2.6×10^{-16}	[27]
R92	$He_2^* + O_3 \rightarrow 2He + O + e + O_2^+$	3.6×10^{-16}	[27]
R93	$O^- + O_3 \rightarrow O + O_3^-$	$1.99 \times 10^{-16} T_0^{0.5}$	[27]
R94	$O_2^- + O_2 \rightarrow O + O_3^-$	3.5×10^{-21}	[27]
R95	$O_2^- + O_3 \rightarrow O_2 + O_3^-$	$6 \times 10^{-16} T_0^{0.5}$	[27]
R96	$O_3^- + He \rightarrow He + O + O_2 + e$	3×10^{-16}	[27]
R97	$O_3^- + He^* \rightarrow He + O_3 + e$	3×10^{-16}	[27]
R98	$O_3^- + He_2^* \rightarrow 2He + O + O_2 + e$	3×10^{-16}	[27]
R99	$O_3^- + O \rightarrow 2O_2 + e$	1×10^{-17}	[27]
R100	$O_3^- + O \rightarrow O_2 + O_2^-$	$2.5 \times 10^{-16} T_0^{0.5}$	[27]
R101	$O_3^- + O_2^+ \rightarrow 2O + O_3$	1×10^{-13}	[27]
R102	$O_3^- + O_2^+ \rightarrow O_2 + O_3$	$2 \times 10^{-13} T_0^{-1}$	[27]
R103	$O_3^- + He + He_2^+ \rightarrow 3He + O_3$	$2 \times 10^{-37} T_0^{-2.5}$	[27]
R104	$O_3^- + O_2 + He_2^+ \rightarrow 2He + O_3 + O_2$	$2 \times 10^{-37} T_0^{-2.5}$	[27]
R105	$O_3^- + O_3 \rightarrow 3O_2 + e$	1×10^{-16}	[27]
R106	$O^- + 2O_2 \rightarrow O_2 + O_3^-$	$1.1 \times 10^{-42} T_0^{-1}$	[27]
R107	$O^- + He + O_2 \rightarrow He + O_3^-$	$1 \times 10^{-42} T_0^{-1}$	[27]
R108	$O + He^+ \rightarrow He + O^+$	$5 \times 10^{-17} T_0^{0.5}$	[27]
R109	$O_2 + He^+ \rightarrow He + O + O^+$	$1.07 \times 10^{-15} T_0^{0.5}$	[27]
R110	$O_3 + He^+ \rightarrow He + O_2 + O^+$	$1.07 \times 10^{-15} T_0^{0.5}$	[27]

R111	$O + He_2^+ \rightarrow 2He + O^+$	$1 \times 10^{-15} T_0^{0.5}$	[27]
R112	$O_2 + He_2^+ \rightarrow 2He + O + O^+$	1.05×10^{-15}	[27]
R113	$O_3 + He_2^+ \rightarrow 2He + O_2 + O^+$	$1 \times 10^{-15} T_0^{0.5}$	[27]
R114	$O_2 + O+ \rightarrow O + O_2+$	$2 \times 10^{-17} T_0^{-0.4}$	[27]
R115	$O_3 + O+ \rightarrow O_2 + O_2^+$	1×10^{-16}	[27]
R116	$He^* + O_2+ \rightarrow O + He + O^+$	1×10^{-26}	[27]
R117	$He_2^* + O_2+ \rightarrow O + 2He + O^+$	1×10^{-16}	[27]
R118	$He_2^* + He \rightarrow 3He$	4.9×10^{-22}	[27]
R119	$He^* + O \rightarrow He + e + O^+$	2.6×10^{-16}	[27]
R120	$O + He + O^+ \rightarrow He + O_2^+$	$1 \times 10^{-41} T_0^{0.5}$	[27]
R121	$O + O_2 + O^+ \rightarrow O_2 + O_2^+$	$1 \times 10^{-41} T_0^{0.5}$	[27]
R122	$He + He^* + O \rightarrow 2He + e + O^+$	1×10^{-43}	[27]
R123	$He + He^* + O_3 \rightarrow 2He + O + e + O_2^+$	1.6×10^{-43}	[27]
R124	$He + O + H \rightarrow He + OH$	$3.2 \times 10^{-45} T_0^{-1}$	[27]
R125	$O^- + O^+ \rightarrow 2O$	$2.7 \times 10^{-13} T_0^{-0.5}$	[27]
R126	$O_2^- + O^+ \rightarrow O + O_2$	$2 \times 10^{-13} T_0^{-1}$	[27]
R127	$O_3^- + O^+ \rightarrow O + O_3$	$2 \times 10^{-13} T_0^{-1}$	[27]
R128	$O^- + He + O^+ \rightarrow He + 2O$	$2 \times 10^{-37} T_0^{-2.5}$	[27]
R129	$O^- + O_2 + O^+ \rightarrow O_2 + 2O$	$2 \times 10^{-37} T_0^{-2.5}$	[27]
R130	$O^- + O_2 + O^+ \rightarrow 2O_2$	$2 \times 10^{-37} T_0^{-2.5}$	[27]
R131	$O_2^- + He + O^+ \rightarrow He + O + O_2$	$2 \times 10^{-37} T_0^{-2.5}$	[27]
R132	$O_2^- + O_2 + O^+ \rightarrow 2O_2 + O$	$2 \times 10^{-37} T_0^{-2.5}$	[27]
R133	$O_2^- + O_2 + O^+ \rightarrow O_2 + O_3$	$2 \times 10^{-37} T_0^{-2.5}$	[27]
R134	$O_3^- + He + O^+ \rightarrow He + O + O_2$	$2 \times 10^{-37} T_0^{-2.5}$	[27]
R135	$O_3^- + O_2 + O^+ \rightarrow O_3 + O + O_2$	$2 \times 10^{-37} T_0^{-2.5}$	[27]
R136	$O_3^- + He + O_2^+ \rightarrow O_3 + He + O_2$	$2 \times 10^{-37} T_0^{-2.5}$	[27]
R137	$O_3^- + O_2 + O_2^+ \rightarrow O_3 + 2O_2$	$2 \times 10^{-37} T_0^{-2.5}$	[27]

All rate coefficients have units of $m^3 s^{-1}$ for two body reactions and $m^6 s^{-1}$for three body reactions. ε_{ave} is the average electron energy in eV; T_e is the electron temperature in eV; T_{eg} is the normalized electron temperature to gas temperature, $T_{eg} = T_e / T_g$; T_0 is the normalized gas temperature to 300 K, $T_0 = (T[k])/(300[K])$.

References

[1] D. Wang and T. Namihira, "Nanosecond pulsed streamer discharges: II. physics, discharge characterization and plasma processing," *Plasma Sources Science and Technology*, vol. 29, p. 023001, feb 2020. 1

[2] T. Huiskamp, F. J. C. M. Beckers, W. F. L. M. Hoeben, E. J. M. van Heesch, and A. J. M. Pemen, "Matching a (sub)nanosecond pulse source to a corona plasma reactor," *Plasma Sources Science and Technology*, vol. 25, p. 054006, sep 2016. 1

[3] P. Sunka, V. Babický, M. Clupek, P. Lukes, M. Simek, J. Schmidt, and M. Cernák, "Generation of chemically active species by electrical discharges in water," *Plasma Sources Science and Technology*, vol. 8, pp. 258–265, jan 1999. 1

[4] S. M. Starikovskaia, "Plasma-assisted ignition and combustion: nanosecond discharges and development of kinetic mechanisms," *Journal of Physics D: Applied Physics*, vol. 47, p. 353001, aug 2014. 1

[5] H. Ayan, D. Staack, G. Fridman, A. Gutsol, Y. Mukhin, A. Starikovskii, A. Fridman, and G. Friedman, "Application of nanosecond-pulsed dielectric barrier discharge for biomedical treatment of topographically non-uniform surfaces," *Journal of Physics D: Applied Physics*, vol. 42, p. 125202, may 2009. 1

[6] J. L. Walsh, J. J. Shi, and M. G. Kong, "Contrasting characteristics of pulsed and sinusoidal cold atmospheric plasma jets," *Applied Physics Letters*, vol. 88, no. 17, p. 171501, 2006. 1, 3

[7] R. Brandenburg, P. J. Bruggeman, and S. M. Starikovskaia, "Fast pulsed discharges," *Plasma Sources Science and Technology*, vol. 26, p. 020201, jan 2017. 1

[8] G. J. Boyle, M. J. E. Casey, D. G. Cocks, R. D. White, and R. J. Carman, "Thermalisation time of electron swarms in xenon for uniform electric fields," *Plasma Sources Science and Technology*, vol. 28, p. 035009, mar 2019. 1, 3

[9] B. Shizgal, D. R. McMahon, and L. A. Viehland, "Thermalization of electrons in gases," *International Journal of Radiation Applications and Instrumentation. Part C. Radiation Physics and Chemistry*, vol. 34, no. 1, pp. 35 – 50, 1989. 1

[10] J. M. Warman, U. Sowada, and M. P. De Haas, "Transient negative mobility of hot electrons in gaseous xenon," *Phys. Rev. A*, vol. 31, pp. 1974–1976, Mar. 1985. 1

[11] R. Winkler and J. Wilhelm, "Solution of the non-stationary electron boltzmann-equation for a weakly ionized collision dominated plasma," *Computer Physics Communications*, vol. 20, no. 1, pp. 113 – 118, 1980. 1

[12] I. K. Bronic and M. Kimura, "Electron thermalization in rare gases and their mixtures," *The Journal of Chemical Physics*, vol. 104, no. 22, pp. 8973–8988, 1996. 1, 2.1, 3

[13] D. Loffhagen and R. Winkler, "Multi-term treatment of the temporal electron relaxation in he, xe and plasmas," *Plasma Sources Science and Technology*, vol. 5, pp. 710–719, nov 1996. 1

[14] D. Trunec, P. Å panÄl, and D. Smith, "The influence of electronâelectron collisions on electron thermalization in he and ar afterglow plasmas," *Chemical Physics Letters*, vol. 372, no. 5, pp. 728 – 732, 2003. 1, 2.1

[15] S. V. Avtaeva, "Model of the pulsed periodic discharge in Ar-S2 mixtures," in *XIV International Conference on Pulsed Lasers and Laser Applications* (V. F. Tarasenko, A. V. Klimkin, and M. V. Trigub, eds.), vol. 11322, pp. 445 – 451, International Society for Optics and Photonics, SPIE, 2019. 1

[16] A. Sharma, V. Subramaniam, E. Solmaz, and L. L. Raja, "Fully coupled modeling of nanosecond pulsed plasma assisted combustion ignition," *Journal of Physics D: Applied Physics*, vol. 52, p. 095204, dec 2018.

[17] N. Y. Babaeva, D. V. Tereshonok, and G. V. Naidis, "Fluid and hybrid modeling of nanosecond surface discharges: effect of polarity and secondary electrons emission," *Plasma Sources Science and Technology*, vol. 25, p. 044008, jul 2016.

[18] S. Y. Xu, J. S. Cai, and J. Li, "Modeling and simulation of plasma gas flow driven by a single nanosecond-pulsed dielectric barrier discharge," *Physics of Plasmas*, vol. 23, no. 10, p. 103510, 2016.

[19] J. Poggie, "Multi-fluid modelling of pulsed discharges for flow control applications," *International Journal of Computational Fluid Dynamics*, vol. 29, no. 2, pp. 180–191, 2015.

[20] S. Nagaraja, V. Yang, and I. Adamovich, "Multi-scale modelling of pulsed nanosecond dielectric barrier plasma discharges in plane-to-plane geometry," *Journal of Physics D: Applied Physics*, vol. 46, p. 155205, mar 2013. 1

[21] G. J. M. Hagelaar and L. C. Pitchford, "Solving the boltzmann equation to obtain electron transport coefficients and rate coefficients for fluid models," *Plasma Sources Sci. Technol.*, vol. 14, no. 4, pp. 722–733, 2005. 1, 2.1, 2.1, 2.2

[22] Yu. P. Raizer, *Gas Discharge Physics*. Berlin: Springer, 1991. 2.1, 2.1

[23] Z. Ristivojevic and Z. L. Petrović, "A monte carlo simulation of ion transport at finite temperatures," *Plasma Sources Science and Technology*, vol. 21, p. 035001, may 2012. 2.2

[24] A. V. Phelps. Phelps database, LXCat (11/02/2020). 2.2, 1, 2

[25] S. Kelly and M. M. Turner, "Power modulation in an atmospheric pressure plasma jet," *Plasma Sources Science and Technology*, vol. 23, p. 065012, aug 2014. 1, 2

[26] Q. Wang, D. J. Economou, and V. M. Donnelly, "Simulation of a direct current microplasma discharge in helium at atmospheric pressure," *Journal of Applied Physics*, vol. 100, no. 2, p. 023301, 2006. 2.3

[27] M. I. Hasan and J. W. Bradley, "Computational study of the afterglow in single and sequential pulsing of an atmospheric-pressure plasma jet," *Plasma Sources Science and Technology*, vol. 24, p. 055015, sep 2015. 2.3, 5, 2

[28] N. A. Popov, "Pulsed nanosecond discharge in air at high specific deposited energy: fast gas heating and active particle production," *Plasma Sources Science and Technology*, vol. 25, p. 044003, may 2016. 3

[29] D. Z. Pai, D. A. Lacoste, and C. O. Laux, "Nanosecond repetitively pulsed discharges in air at atmospheric pressureâthe spark regime," *Plasma Sources Sci. Technol.*, vol. 19, no. 065015, 2010. 3

[30] D. L. Rusterholtz, D. Z. Pai, G. D. Stancu, D. A. Lacoste, and C. O. Laux, "Ultrafast heating in nanosecond discharges in atmospheric pressure air," in *50th Aerospace Sciences Meeting (American Institute of Aeronautics and Astronautics, Reston, VA)*, 2012. 3